The Journal of Nutrition 156 (2026) 101774

THE JOURNAL OF NUTRITION

journal homepage: https://jn.nutrition.org/

Nutrition and Disease

Persistent Lipotoxicity Overwhelms Adaptive Capacity in Human Hepatic Cell Line

Ilaria Serra [1,2], Elisa Bisconti [2], Francesco Vari [2], Eleonora Stanca [3], Federica De Castro [2], Federica Angilè [2], Daniele Vergara [2], Francesco Paolo Fanizzi [2], Anna M Giudetti [2,*]

[1] *Department of Physiology and Pharmacology "V. Erspamer", Sapienza University of Rome, Rome, Italy;* [2] *Department of Biological and Environmental Sciences and Technologies (DiSTeBA), University of Salento, Lecce, Italy;* [3] *Department of Experimental Medicine, University of Salento, Lecce, Italy*

A B S T R A C T

Background: Chronic fatty acid (FA) elevation drives metabolic dysfunction-associated steatotic liver disease. Hepatocytes buffer transient lipid overload via coordinated adaptive mechanisms, but the temporal limits of this capacity remain undefined.
Objectives: We characterized early, intermediate, and prolonged hepatocellular responses to sustained lipid excess.
Methods: HuH7 hepatocytes were exposed to an equimolar palmitic/oleic acid (PA/OA) mixture for 1, 14, or 28 d. Viability, lipid accumulation, stress-response pathways, insulin signaling, metabolic regulators, mitochondrial markers, [^{14}C]-PA uptake, and exometabolomic profiles were assessed ($n \geq 3$/group). Data (mean ± standard error of the mean) were analyzed by 2-way analysis of variance with Bonferroni post hoc testing; cumulative cell death was analyzed by linear regression. $P < 0.05$ was considered significant.
Results: FA treatment increased lipid droplet accumulation 1.4- to 1.7-fold compared with time-matched bovine serum albumin controls at all time points ($P < 0.001$) and increased the rate of cumulative cell death ~4.3-fold (1.556% ± 0.083% compared with 0.365 ± 0.054%/d, $P < 0.001$). Exometabolomic principal component analysis explained 88.5% of variance ($Q^2 = 0.758$), with peak lactate release at day 14 and progressively rising acetate through day 28. [^{14}C]-PA accumulation at day 28 was ~30% lower than day 1 (~800 compared with ~500 cpm/mg protein), with a declining rather than plateauing profile between 20 and 60 s. By day 28, FA-treated cells showed lower FA synthase ($P < 0.001$), CD36 ($P < 0.05$), FABP1 ($P < 0.001$), SIRT1 ($P < 0.005$), and CLOCK ($P < 0.01$) protein levels, and higher carnitine palmitoyl transferase 1A ($P < 0.001$), phosphorylated AMP-activated protein kinase (AMPK)/AMPK ($P < 0.01$), p53 ($P < 0.001$), Bax/Bcl2 ($P < 0.005$), and respiratory complex I-V abundance ($P < 0.05$–$P < 0.001$) compared with controls.
Conclusions: Sustained PA/OA exposure induces a staged hepatocellular response, early lipid-buffering adaptation, intermediate metabolic compensation, and late decompensation, indicating that chronic lipotoxicity reflects progressive loss of regulatory coordination despite persistent metabolic adaptation.

Keywords: oleic acid, palmitic acid, lipotoxicity, adaptive failure, hepatocytes

Introduction

The liver stands at the metabolic crossroads of systemic energy homeostasis, continuously orchestrating the uptake, synthesis, oxidation, and storage of fatty acids (FAs) in response to fluctuating nutrient availability [1]. Under physiological conditions, hepatocytes exhibit remarkable plasticity, efficiently buffering transient elevations in circulating FAs through coordinated metabolic reprogramming and stress mitigation pathways. However, obesity and metabolic disorders expose hepatocytes to sustained lipid overload, which contributes to metabolic dysfunction-associated steatotic liver disease (MASLD) [2]. MASLD affects >30% of the global population and represents a major cause of chronic liver disease [3]. Its progression from steatosis to steatohepatitis, fibrosis, and cirrhosis reflects, at least in part, the inability of hepatocytes to maintain

Abbreviations: AMPK, AMP-activated protein kinase; BSA, bovine serum albumin; CAT, catalase; CPT1A, carnitine palmitoyl transferase 1A; ER, endoplasmic reticulum; FASN, fatty acid synthase; FA, fatty acid; FAO, fatty acid oxidation; GPx-4, glutathione peroxidase-4; HKII, hexokinase II; LD, lipid droplet; MASLD, metabolic dysfunction-associated steatotic liver disease; OA, oleic acid; OPLS-DA, orthogonal partial least square-discriminant analysis; PA, palmitic acid; PCA, principal component analysis; ROS, reactive oxygen species; SOD1, superoxide dismutase 1.

* Corresponding author. *E-mail address:* anna.giudetti@unisalento.it (A.M. Giudetti).

https://doi.org/10.1016/j.tjnut.2026.101774
Received 23 January 2026; Received in revised form 13 July 2026; Accepted 3 August 2026; Available online 7 August 2026

adaptive responses under prolonged metabolic stress [4]. Despite extensive research into lipotoxicity, how hepatocytes transition from lipid adaptation to maladaptive injury during persistent FA exposure remains incompletely understood.

Among circulating FAs, palmitic acid (PA, 16:0) is a potent inducer of lipotoxic stress, promoting endoplasmic reticulum (ER) stress, oxidative stress, and proapoptotic signaling [5]. In contrast, oleic acid (OA, 18:1) can attenuate PA-induced toxicity by promoting triacylglycerol synthesis and lipid droplet (LD) formation, thereby diverting FAs away from toxic lipid intermediates [6]. PA and OA are major FAs incorporated into liver triacylglycerols, and the balance between SFA and MUFA influences hepatocellular lipotoxicity and MASLD progression [7,8]. Consistently, in vitro studies have shown that OA cotreatment reduces PA-induced cytotoxicity, ER stress, and apoptosis during acute exposure, supporting the role of OA-mediated esterification in lipid buffering [9,10].

Most in vitro models focus on acute FA exposure, typically 16 to 24 h, and therefore capture early cellular responses to lipid excess. However, in patients, hepatocytes are exposed to elevated FA for months or years, requiring sustained rather than transient adaptation. Whether protective mechanisms observed during acute exposure are maintained, remodeled, or progressively lost under chronic lipid stress remains unclear [11,12].

Emerging evidence suggests that hepatocyte resilience under chronic stress depends not only on individual adaptive pathways but on integrated regulatory networks that coordinate metabolism, stress responses, and bioenergetic homeostasis [13]. Among these, the AMP-activated protein kinase (AMPK)–SIRT1 axis has emerged as a primary regulatory node. AMPK, activated by energetic stress, promotes catabolic metabolism by stimulating FA oxidation (FAO), inhibiting lipogenesis, and inducing autophagy [14]. SIRT1, a NAD^+-dependent deacetylase, orchestrates mitochondrial biogenesis, antioxidant defenses, and metabolic flexibility through deacetylation of key transcription factors, including PGC-1α, FOXO, and LXR [15]. Critically, AMPK and SIRT1 engage in reciprocal activation, forming a positive feedback loop essential for sustained metabolic adaptation. Disruption of the AMPK–SIRT1 axis has been implicated in MASLD progression, yet whether chronic lipid exposure directly erodes this regulatory network and whether such erosion contributes to adaptive failure remains unknown [16].

In the present study, we adopted a temporal stress-adaptation framework to investigate hepatocyte responses to sustained lipid overload. Using human HuH7 hepatocytes exposed to a PA/OA mixture (1:1 ratio), we compared early responses (24 h) with those emerging at 14 d and 28 d, a duration far exceeding conventional protocols and designed to reveal the transition from metabolic adaptation to adaptive failure under persistent lipid stress.

By integrating temporal analyses of lipid accumulation, metabolic reprogramming, stress response pathways, bioenergetic signaling, and cell viability, we reveal a progressive uncoupling between compensatory metabolic reprogramming and cellular survival. Our findings demonstrate that sustained activation of adaptive pathways, including increased CPT1A expression, AMPK signaling, and autophagy, occurs paradoxically alongside declining SIRT1 expression, antioxidant depletion, dysregulated ER stress, and mounting cell death, indicating that metabolic adaptation alone cannot ensure long-term hepatocyte resilience. These results highlight critical temporal transitions in cellular stress responses that may inform therapeutic strategies aimed at sustaining hepatocyte resilience during chronic metabolic lipid overload.

Methods

Cell cultures and reagents

Human hepatocellular carcinoma HuH7 cells (cat. #JCRB0403, purchased from Japanese Cancer Research Resources Bank, JCRB) were maintained in low-glucose (1 g/L glucose, corresponding to ~5.5 mM glucose) Dulbecco's Modified Eagle Medium (DMEM, Sigma-Aldrich D5546) supplemented with 10% fetal bovine serum (Capricorn HI-12A), penicillin/streptomycin (Sigma-Aldrich #P4333), and glutamine (Sigma-Aldrich G7513), under standard culture conditions (37 °C, 5% CO_2). HuH7 cells were selected as a well-characterized hepatic cell model frequently used to study lipid handling and metabolic stress responses, while acknowledging their transformed origin and associated metabolic adaptations. PA (Cat. no. 506345) and OA (Cat. no. 75090) were conjugated to FA-free bovine serum albumin (BSA, Cat. no. 03117057001) at a molar ratio of ~2:1 (FA:BSA), comparable with physiological albumin-binding conditions in circulation [17]. FAs were freshly prepared and diluted in culture medium immediately before use to minimize spontaneous oxidation. To assess insulin responsiveness, HuH7 cells were serum-starved for 4 h. Thereafter, cells were acutely treated with 100 nM insulin (Sigma-Aldrich) for 10 min and immediately lysed for protein extraction. This insulin concentration was selected to provide a robust and reproducible activation of the insulin pathway [18].

FA treatments and experimental design

Cells were exposed to a PA/OA mixture (1:1 molar ratio; final concentration 0.2 mM total FAs) or to BSA alone as a carrier control. This FA concentration was selected to induce lipid overload while avoiding acute cytotoxicity. The 1:1 PA/OA ratio was chosen because it is widely adopted in the literature for in vitro models of FA overload [19–21] and is consistent with our previous work [6,18,22,23]. During treatments, cells were maintained in the same low-glucose DMEM formulation described previously, and culture medium containing BSA or FA was refreshed every 48 to 72 h. To preserve culture viability over extended periods, cells were periodically passaged and reseeded at defined densities. We recognize that repeated passaging introduces selective pressure; accordingly, the prolonged exposure paradigm is interpreted as a stress-adaptation model rather than a direct disease mimic. Cell viability was monitored throughout the exposure period using Trypan Blue exclusion assays, and cumulative cell death was calculated as a percentage of total counted cells [24].

BODIPY staining

To visualize LD accumulation, cells were seeded 2 d before staining into 6-well plates containing sterile glass coverslips, at a density of 2×10^5 cells/well. Both day 1 and day 28 (maintaining chronic treatment with BSA or PA/OA) were prepared in parallel. For day 1 condition, HuH7 cells were treated the next day with either FA-free BSA (control) or a PA/OA mixture (0.2

mM final concentration, 1:1 molar ratio). After 24 h of treatment, both day 1 and day 28 cells were washed twice with phosphate-buffered saline (PBS) and fixed with 4% paraformaldehyde for 15 min at room temperature. After fixation, all samples were incubated with BODIPY 493/503 at a dilution of 1:1000 in PBS from a stock solution of 1 mg/mL for 15 min at room temperature in the dark to stain neutral lipids. Coverslips were mounted onto glass slides, and images were captured using a Cell Imaging Station microscope (Invitrogen, FLoid Cell Imaging Station, 10 213-412, Thermo Fisher Scientific) at 20× magnification with a scale bar of 100 μm. Absorbance was measured at 570 nm by a Biotek Cytation 5 Cell Imaging Multimode Reader (Agilent Technologies) and normalized on total cell number.

Western blotting analysis

Proteins were extracted from cells using the radioimmunoprecipitation assay lysis buffer (cat. no. 9806, Cell Signaling). The Bradford method was used to quantify total protein levels (BIO-RAD). Proteins were separated by SDS-polyacrylamide gel electrophoresis and transferred onto a nitrocellulose membrane (Bio-Rad Laboratories). After blocking at room temperature for 1 h with 5% (w/v) skim milk in TBS-Tween buffer (Tris-buffered saline plus 0.5% (v/v) Tween-20, TTBS), membranes were incubated with primary antibodies (the list of primary antibodies used is reported in Supplemental Table 1). After washing with TTBS, blots were incubated with peroxidase-conjugated secondary antibodies (cat. no. A3687 and cat no. A3652, Sigma-Aldrich) at 1:10,000 dilutions at room temperature for 1 to 2 h. The filters were then washed twice in TTBS. Western blotting analyses were performed using the Amersham ECL Advance Western Blotting Detection Kit (cat. no. RPN2106, GE Healthcare). Densitometric analysis of immunoblots was performed using Image Lab software version 6.0.1 2017 (Bio-Rad Laboratories, Inc.). Red Ponceau staining was used as the protein loading control.

Kinetic of [U-^{14}C] -palmitate uptake

Time-dependent uptake of radiolabeled palmitate was assessed by using the assay described by Stremmel and Berk [25]. Briefly, HuH7 cells maintained under FA treatment for 1 or 28 d were washed with PBS and incubated at 37 °C with prewarmed [U-^{14}C]-palmitate solution containing 100 μM [U-^{14}C]-PA and 100 μM FA-free BSA in PBS, with a specific activity of 40 mCi/mmol. Uptake was measured at 10, 20, 40, and 60 s. At each time point, uptake was rapidly stopped by aspirating the solution and washing the cells with ice-cold PBS containing 0.5% BSA to remove extracellular and membrane-associated palmitate. Cells were then lysed in 1 M NaOH, and aliquots of the lysates were used for radioactivity measurement by liquid scintillation counting. Radioactivity values were normalized to total protein content and expressed as counts per minute per milligram (cpm/mg) protein.

Metabolomic analysis by ^{1}H- Nuclear Magnetic Resonance

According to previously reported procedures [26,27], the recovered culture media (900 μL) was mixed with 100 μL buffer [1.5 M K2HPO4, 2 mM trimethylsilyl propionate (TSP), and 2 mM sodium azide, at pH 7.4] to minimize variations in metabolite nuclear magnetic resonance (NMR) chemical shifts. Samples were then vortexed and centrifuged. The supernatants (600 μL) were finally placed in 5 mm outer diameter NMR tubes.

All measurements were recorded on the Bruker Avance spectrometer (Bruker) operating at 400.13 MHz, T = 300 K, equipped with a PABBI 5-mm inverse detection probe incorporating a z-axis gradient coil. A time delay of 5 min was set between sample injection and preacquisition calibrations to ensure complete temperature equilibration (300 K). Experiments were run in automation mode after loading individual samples on a Bruker Automatic Sample Changer, interfaced with the software Icon NMR (Bruker).

A 1-dimensional CPMG experiment with a transverse-relaxation-filter incorporating pulse sequence (referred to as Carr-Purcell-Meiboom-Gill spin-echo sequence, CMPG) was run with 256 scans, a total spin-spin relaxation delay of 20 μs, and solvent signal saturation during the relaxation delay. The FIDs were multiplied by an exponential weighting function corresponding to a line broadening of 0.3 Hz before Fourier transformation, phasing, and baseline correction. All spectra were referenced to the TSP signal (δ = 0.00 ppm). The metabolites were assigned based on Chenomx Suite V 12 and comparison with the Human Metabolome Database and other published data [28].

Spectral processing and multivariate data analysis

^{1}H-CPMG NMR spectra were automatically divided into rectangular buckets of fixed 0.04 ppm width and integrated using Bruker Amix 3.9.13 (Bruker BioSpin) software. The spectral region between 4.5 and 5 ppm (residual protic water signal) was discarded to exclude the effects of variability in the water suppression signal. The remaining buckets in the range of 10.00 to 0.50 ppm were normalized to total area to minimize small differences and subsequently mean-centered. The Pareto scaling method, which is performed by dividing the mean-centered data by the square root of the SD, was then applied to the variables. Multivariate statistical analyses were performed with the software SIMCA-P (V14, Umetrics). Principal component analysis (PCA), an unsupervised pattern recognition method, was performed to identify general metabolic trends and possible outliers. Then, orthogonal partial least square-discriminant analysis (OPLS-DA), a supervised multivariate data analysis, was carried out to improve the statistically significant metabolite variations related to complex exposures. The statistical models' (PCA and OPLS-DA) performance was evaluated by R2(cum) and Q2(cum) parameters for goodness of fit and prediction, respectively, according to 7-fold internal cross-validation, further evaluated with a permutation test (100 permutations) of SIMCA-P software [29].

Determination of intracellular reactive oxygen species by 2',7'-dichlorodihydrofluorescein diacetate assay

Intracellular reactive oxygen species (ROS) levels were assessed using the cell-permeable fluorescent probe 2',7'-dichlorodihydrofluorescein diacetate (DCFH-DA, D399). HuH7 cells were seeded in 12-well plates and subjected to either acute

(24 h) or chronic (28 d) exposure to FA as described in the experimental design. A vehicle-treated group (BSA) served as the control for both time points. At the end of the incubation periods, cells were washed with PBS and incubated with a fresh serum-free culture medium containing 20 μM DCFH-DA for 30 min at 37°C, in the dark. After incubation, cells were washed twice with PBS to remove the extracellular dye and resuspended in PBS for imaging. Images were captured using a fluorescence microscope (Cell Imaging Station microscope, Invitrogen, FLoid Cell Imaging Station, 10 213–412, Thermo Fisher Scientific) at 20× magnification with a scale bar of 100 μm, and the mean fluorescence intensity, proportional to ROS production, was quantified using ImageJ software (NIH).

RNA extraction and real-time PCR analyses

Total RNA was extracted with TRI reagent (Zymo Research, R2050-1). RNA quantification was performed using a NanoDrop One Spectrophotometer (Thermo Fisher Scientific). Gene expression analyses were performed through real-time PCR using SYBR Green technology (FluoCycle, Euroclone), run on CFX Connect Real-Time System (Bio-Rad Laboratories). GAPDH was used as a housekeeping gene, and the relative expression levels were expressed as fold change. The list of primers is reported in Supplemental Table 2.

Statistical analysis

Data are presented as mean ± SEM from ≥3 independent experiments. Statistical significance was assessed using 2-way analysis of variance, with time and treatment as factors, followed by Bonferroni post hoc testing. A P value of <0.05 was considered statistically significant. For proportional data expressed as fold change, values were log2-transformed before statistical analysis and visualization to represent reciprocal increases and decreases on an equivalent scale. For the longitudinal cell death analysis, cumulative cell death was analyzed by simple linear regression. Slopes were compared between BSA- and FA-treated cells, and the accumulation rate was reported as % cell death/d. All statistical analyses were performed using GraphPad Prism 9.1.0.

Results

Temporal dissociation between lipid storage capacity and cell viability under chronic FA exposure

To characterize the time-dependent responses to lipid overload, HuH7 cells were exposed to a PA/OA mixture at an equimolar ratio for 24 h, 14 d, and 28 d. Across all time points, FA-treated cells displayed persistent intracellular LD accumulation, as visualized by BODIPY staining (Figure 1A, B), indicating that the capacity for neutral lipid storage is maintained throughout the entire exposure period regardless of treatment duration.

Despite this sustained lipid accumulation, the trajectory of cell viability diverged markedly over time. At day 1, cell morphology and viability remained intact, indicating effective buffering of lipid stress during this early phase (Figure 1C, D). At day 14, phase-contrast microscopy similarly did not reveal marked alterations in cell shape or overt morphological deterioration (Figure 1C, D). In contrast, on day 28, cellular homeostasis was altered, resulting in mounting cytotoxicity. Linear regression analysis of cumulative cell death (Figure 1D) showed that FA treatment markedly increased the rate of cell death compared with BSA controls, with an accumulation rate of 1.556% ± 0.083% cell death/d in FA-treated cells compared with 0.365% ± 0.054% cell death/d in BSA-treated cells, corresponding to a ∼4.3-fold higher rate under FA exposure. This cumulative toxicity was accompanied by profound morphological deterioration, with cells becoming progressively enlarged and rounded, with diminished confluence, hallmarks of chronic metabolic stress and compromised cellular integrity (Figure 1C). These pathological features were absent in BSA-treated controls, although prolonged culture alone induced modest baseline changes, underscoring the importance of time-matched controls in chronic exposure models.

By ^{1}H-NMR spectroscopy, we analyzed the exometabolome (i.e., the cell culture media) to obtain valuable information on the physiological state of the cells [26,30]. The principal metabolites that allow for defining clusters included glucose, a range of amino acids (glutamine, valine, isoleucine, leucine, tyrosine, and phenylalanine), acetate, lactate, pyruvate, myoinositol, and glutamate (Figure 1E, F).

As an initial, unsupervised approach, PCA was applied to the bucketed ^{1}H CPMG NMR spectra obtained from culture media across all experimental conditions (Figure 1). The PCA model revealed a marked separation along the first principal component (t[1]) between day 1 (BSA-1 and FA-1) and those collected at later time points (days 14 and 28), consistent with higher medium glucose content in the day 1 media (Figure 1E). Along the second principal component (t[2]), FA-14 was distinguished by elevated lactate levels (Figure 1F), whereas FA-28 exhibited higher acetate content.

Pairwise OPLS-DA analysis reveals treatment- and time-dependent shifts in extracellular metabolite profiles

To investigate the differences in culture media in greater depth, pairwise supervised OPLS-DA models were constructed, enabling the evaluation of treatment effects (Figure 2A–F) and time-dependent metabolic shifts, within the FA-treated group (Figure 2G–L) and within the BSA group, the latter serving as a reference for natural metabolic drift in BSA-treated cells (Supplemental Figure 1).

All pairwise OPLS-DA models yielded clear metabolite discrimination between experimental groups, as evidenced by consistent sample separation along the predictive component (t[1]) in the score plots (Figure 2A–F). The corresponding S-line plots identified the metabolites driving each separation: positive covariance and correlation values denote metabolites enriched in the class projected onto the positive side of t[1], whereas negative values reflect relative depletion.

Across comparisons, glucose, tyrosine, pyruvate, glutamine, acetate, lactate, myoinositol, and formate emerged as the primary contributors to class discrimination, each displaying distinct directional changes depending on the contrast examined, and collectively providing a coherent picture of the metabolic shifts characterizing each pairwise comparison.

Relative to their respective controls, FA-1 showed higher glucose and lower pyruvate, acetate, lactate, glutamine, and

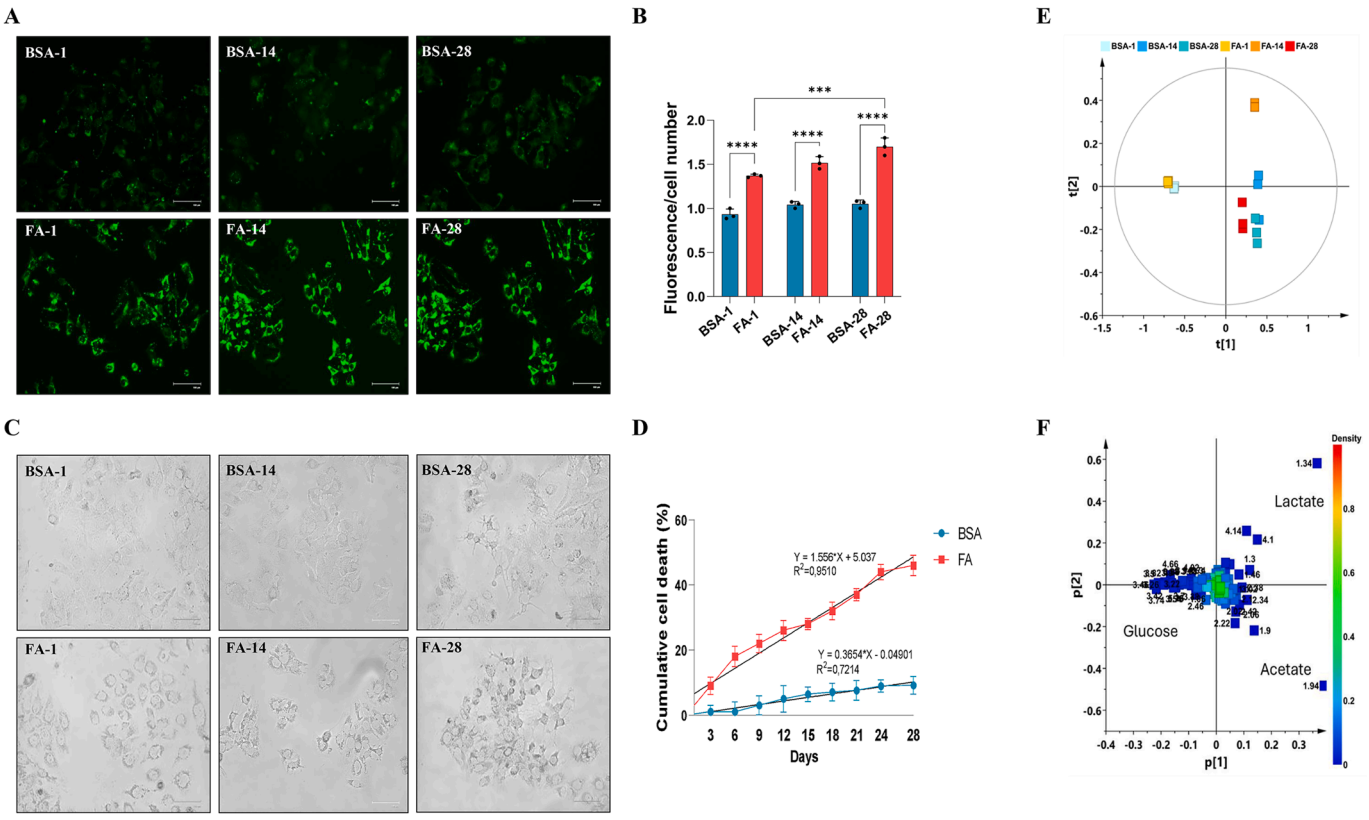

FIGURE 1. Fatty acid (FA)-induced lipid accumulation and metabolic adaptation in HuH7 cells over time. (A, B) Representative fluorescence microscopy images of HuH7 cells stained with BODIPY 493/503 to visualize lipid droplets after FA treatment at day 1, day 14, and day 28, with corresponding quantification of BODIPY fluorescence intensity. (C) Representative phase-contrast images of control (BSA) and FA-treated HuH7 cells on day 1, day 14, and day 28. Scale bars = 100 μm. (D) Cumulative cell death (%) in BSA- and FA-treated HuH7 cells over time. Linear regression was used to estimate the rate of cell death accumulation. (E, F) Principal component analysis (PCA) (3 components) (R2X = 0.885; Q2 = 0.758) of the recovered cell's culture media (exometabolome). (I) Score plot. (J) Loading plot. Data are presented as mean ± SEM from 3 independent experiments. Quantitative data are expressed as fold change relative to BSA-1 or log2 fold change relative to BSA-1. Statistical significance: $^{*}P < 0.05$; $^{**}P < 0.01$; $^{***}P < 0.005$; $^{****}P < 0.001$. BODIPY, boron-dipyrromethene; BSA, bovine serum albumin.

tyrosine in the conditioned media (Figure 2A, B). FA-14 was associated with higher lactate and myoinositol, alongside lower glutamine, acetate, pyruvate, formate, and tyrosine (Figure 2C, D). FA-28 exhibited higher glucose and tyrosine, with lower acetate, glutamine, and lactate (Figure 2E, F).

Analysis of the OPLS-DA models comparing culture media from FA-treated cells across time points (Figure 2G–L) revealed a progressive accumulation of acetate, with levels increasing steadily from day 1 to day 28. Lactate was elevated in both FA-14 and FA-28 relative to FA-1 (Figure 2G–J), with FA-14 displaying the greatest accumulation. Alanine levels were higher in the conditioned media of FA-14 and FA-28 than in FA-1 and remained largely unchanged between the 2 later time points. In contrast, glucose levels were lower in FA-14 and FA-28 than in FA-1. Notably, the direct comparison between FA-14 and FA-28 revealed higher glucose and lower lactate in FA-28 (Figure 2K, L). The same comparisons were also made between control cells during the time of BSA (Supplemental Figure 1).

Lipid and energetic metabolic reprogramming induced by long-term FA treatment

To follow the adaptive metabolic strategies of hepatocytes during chronic lipid challenge, we examined key regulators governing lipid flux, bioenergetics, and metabolic homeostasis.

At day 1, FA synthase (FASN) and ACC expression were minimally affected by FA exposure (Figure 3A, B), suggesting that early adaptive responses primarily involve lipid storage rather than transcriptional metabolic rewiring. As exposure was prolonged, however, a progressive suppression of de novo lipogenic enzyme expression became evident. FASN protein levels were already markedly reduced at day 14, whereas inhibitory phosphorylation of ACC did not reach significance until day 28, indicating that suppression of lipogenic enzyme expression precedes the full inhibition of ACC activity during sustained FA exposure (Figure 3A, B). These changes were accompanied by corresponding transcriptional reprogramming, as real-time PCR confirmed the downregulation of FASN and ACC at the mRNA level, consistent with transcriptional-mediated suppression of lipogenic targets (Figure 3C).

In parallel, markers of FA trafficking were progressively remodeled. CD36 protein and mRNA expression declined over time, and FABP1 protein levels decreased progressively, with a reduction already evident at day 14 that became more pronounced by day 28 (Figure 3A–C).

To functionally validate whether these molecular changes translate into impaired FA internalization, we performed a kinetic analysis of [U-^{14}C]-PA uptake on day 1 and day 28. On day 1, HuH7 cells exhibited rapid and progressive PA accumulation, reaching ~800 cpm/mg protein at 60 s. At day 28, uptake was

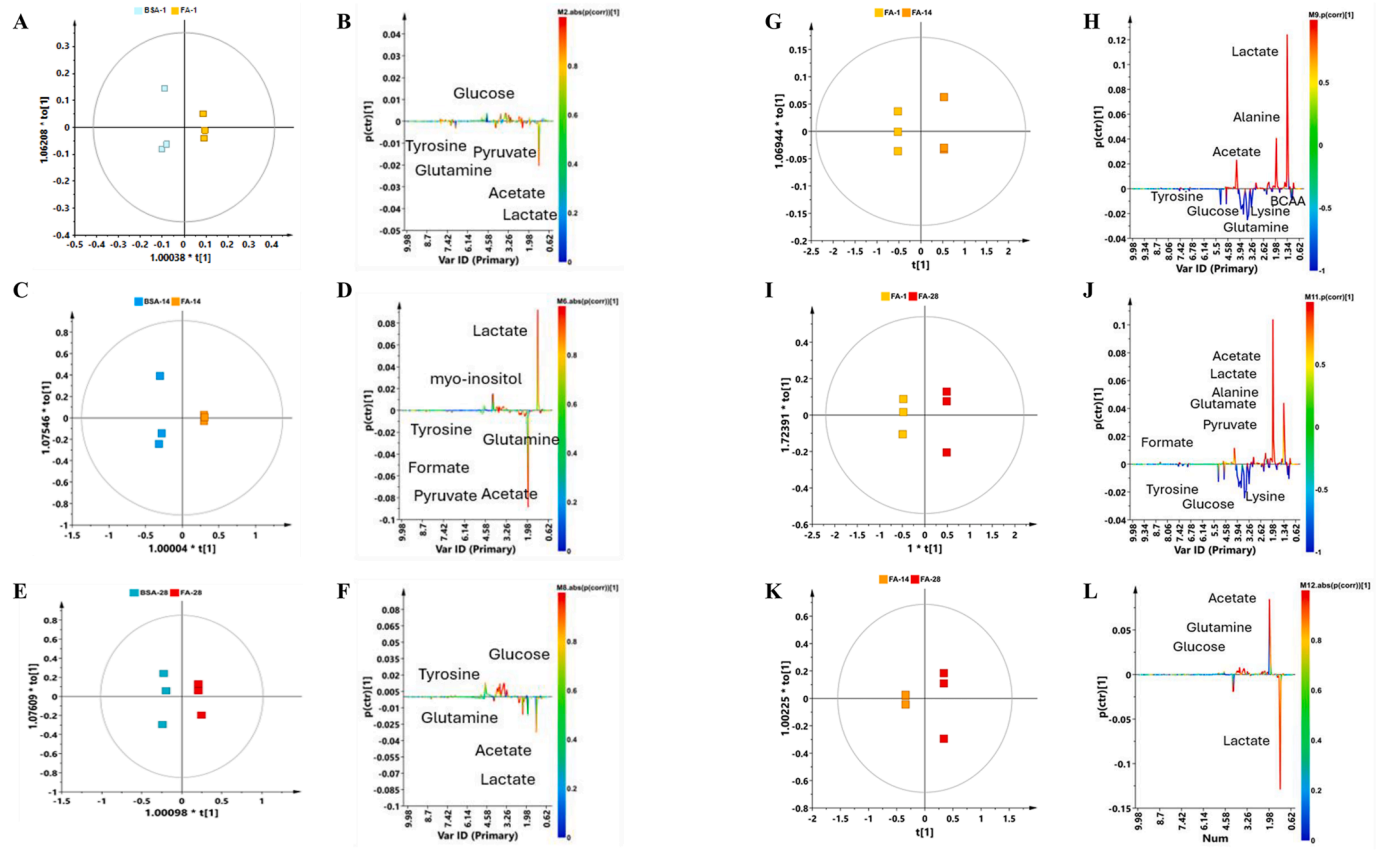

FIGURE 2. Orthogonal partial least square-discriminant analysis (1+1+0), pairwise comparison of the recovered cell's culture media (exo-metabolome). (A, C, E, G, I, K) Score plots. (B, D, F, H, J, L) Loading plots. (A,B) BSA-1 compared with FA-1 ($R^2X = 777$; $R^2Y = 994$; $Q^2 = 965$). (C,D) BSA-14 compared with FA-14 ($R^2X = 954$; $R^2Y = 999$; $Q^2 = 996$). (E,F) BSA-28 compared with FA-28 ($R^2X = 84$; $R^2Y = 992$; $Q^2 = 963$). (G, H) FA-1 compared with FA-14 ($R^2X = 0.99$; $R^2Y = 1$; $Q^2 = 1$). (I,J) FA-1 compared with FA-28 ($R^2X = 0.979$; $R^2Y = 1$; $Q^2 = 1$). (K-L) FA-14 compared with FA-28 ($R^2X = 98$; $R^2Y = 1$; $Q^2 = 1$). BSA, bovine serum albumin; FA, fatty acid.

significantly reduced at all time points, plateauing at ~500 cpm/mg protein, a ~30% reduction relative to day 1 (Figure 3D).

To further characterize the temporal dynamics of FA handling, we analyzed the kinetics of [U-^{14}C]-palmitate accumulation on day 1 and day 28 (Figure 3D). On day 1, cell-associated radioactivity increased rapidly within the first 20 s and remained stable thereafter, reaching a plateau that was maintained for ≤60 s. At day 28, cell-associated radioactivity also peaked at 20 s, but at a substantially lower level than day 1, and subsequently declined between 20 and 60 s rather than reaching a stable plateau. This difference in curve shape, and not only in absolute magnitude, could indicate that the reduced PA accumulation at day 28 cannot be fully accounted for by a simple decrease in influx capacity, but instead is consistent with a condition in which efflux and/or intracellular turnover of the tracer might exceed influx during the later time window.

Consistent with this shift away from lipid anabolism, CPT1A expression was significantly upregulated from day 14 onward, with a further increase at day 28 (Figure 3A, B).

The temporal dynamics of DGAT1 expression further support this reorientation. At day 1, DGAT1 was significantly upregulated at both protein and mRNA levels (Figure 3A–C), consistent with the robust LD accumulation observed during acute FA exposure and reflecting an early channeling of excess FA toward triacylglycerol synthesis. However, DGAT1 expression declined progressively with prolonged exposure, falling significantly below respective time-matched controls at days 14 and 28 (Figure 3A–C), suggesting a loss of esterification capacity under chronic lipid stress. In contrast, DGAT2 expression remained unaffected by FA treatment at both acute and chronic time points, at both protein and mRNA levels (Figure 3A–C), indicating that the 2 DGAT isoforms are differentially regulated during the adaptive response to sustained lipid overload.

Molecular mechanism underlying lipotoxicity during prolonged FA exposition

At the molecular level, the loss of viability at day 28 was paralleled by a shift in apoptotic balance. In the context of fatty liver disease, excess FAs promote hepatocyte death primarily through an imbalance in Bcl2 family proteins [31,32]. Consistent with this paradigm, Bax expression rose after 28 d of FA exposure (Figure 4A, B), indicating proapoptotic signaling during sustained lipid stress. Concurrently, 28 d of FA exposure resulted in profound downregulation of Bcl2, leading to a marked elevation of the Bax/Bcl2 ratio (Figure 4A, B). Further evidence of progressive stress signaling was provided by p53 expression analysis. p53 is a key tumor suppressor coordinating cell cycle arrest, DNA damage response, apoptosis, and

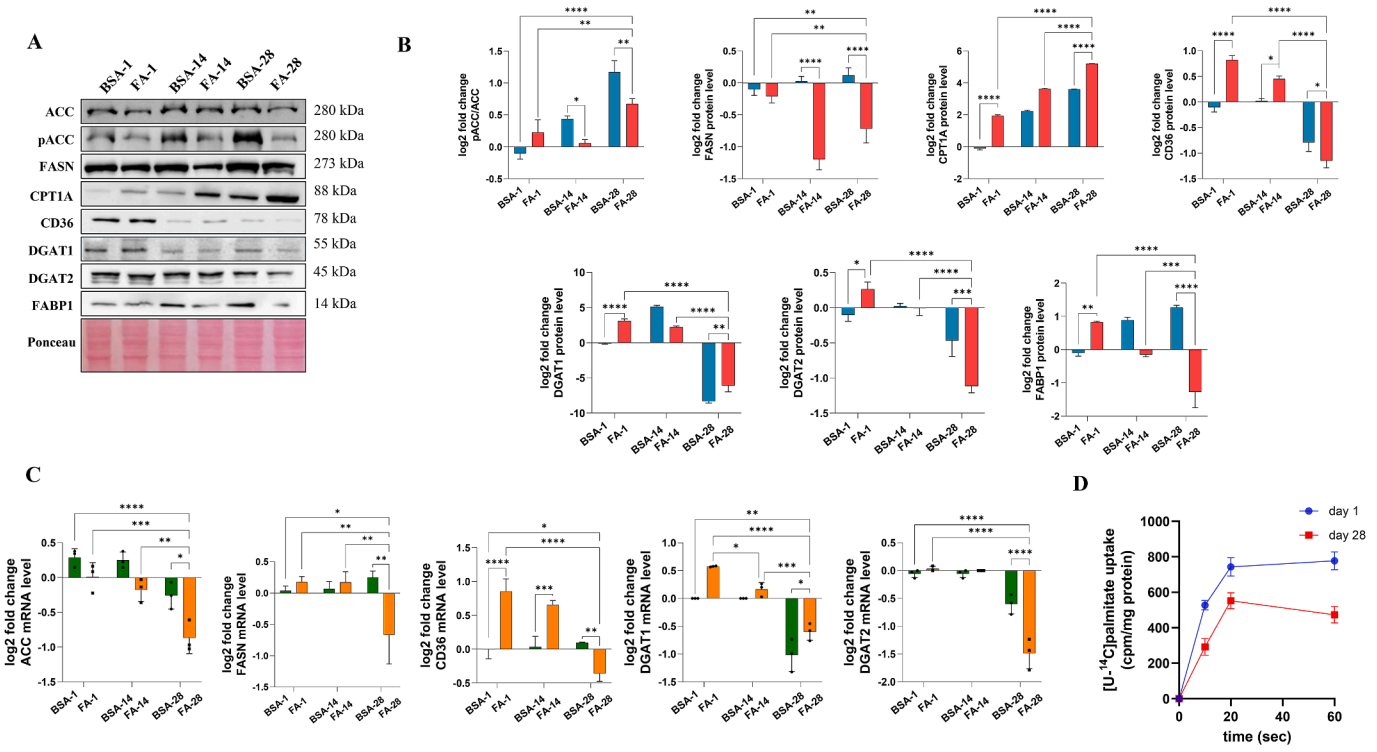

FIGURE 3. Fatty acid (FA) treatment modulates lipogenic, lipid transport, and β-oxidation markers in HuH7 cells. (A) Western blot analysis of ACC, pACC, FASN, CPT1A, CD36, DGAT1, DGAT2, and FABP1, and (B) relative densitometric quantification of pACC/ACC, FASN, CPT1A, CD36, DGAT1, DGAT2, and FABP1 in HuH7 cells treated with BSA or FA at day 1, day 14, and day 28. (C) Relative mRNA expression levels of ACC, FASN, CPT1A, CD36, DGAT1, and DGAT2 at the indicated conditions. (D) Kinetic analysis of [^{14}C]palmitate uptake in HuH7 cells at day 1 and day 28 of FA treatment. Data are presented as mean ± SEM from 3 independent experiments. Quantitative data are expressed as fold change relative to BSA-1 or log2 fold change relative to BSA-1. Statistical significance: *$P < 0.05$; **$P < 0.01$; ***$P < 0.005$; ****$P < 0.001$. ACC, Acetyl-CoA Carboxylase; BSA, bovine serum albumin; CPT1A, carnitine palmitoyl transferase 1A; DGAT, diacylglycerol acyltransferase; FABP1, Fatty Acid-Binding Protein 1; FASN, fatty acid synthase; pACC, phospho Acetyl-CoA Carboxylase.

metabolic regulation, including lipid metabolism and mitochondrial function [33,34]. FA treatment for 1 d resulted in higher p53 protein levels compared with BSA controls, indicating an early stress-responsive induction. After 28 d, p53 levels were further increased in FA-treated cells relative to time-matched controls, suggesting sustained p53 activation under chronic lipid stress (Figure 4A, B). At this later time point, FA-treated cells also displayed a more complex p53 band pattern, consistent with the presence of distinct p53 species previously reported under conditions of chronic cellular stress [35–37].

Prolonged lipid exposition triggers a failure of protective stress responses

To delineate the molecular events underlying the transition from adaptive responses to cellular decompensation, we longitudinally assessed oxidative stress levels, antioxidant defense mechanisms, ER stress responses, and autophagic activity during acute and chronic FA exposure.

ROS levels, measured by DCFH-DA fluorescence, were only modestly elevated after 1 d of FA treatment, whereas prolonged exposure for 28 d resulted in a significant increase in fluorescence intensity compared with both time-matched BSA controls and the 1-d FA condition (Figure 4C, D). This failure of redox control was mirrored by a coordinated, time-dependent collapse of antioxidant enzyme expression.

Acute FA exposure was associated with upregulation of both catalase and glutathione peroxidase-4 (GPx-4) (Figure 4E, F), consistent with an early adaptive antioxidant response to increased FA flux and lipid peroxidation. However, after chronic FA exposure, both enzymes were markedly suppressed below baseline levels, indicating a loss of compensatory redox capacity. GPx-4 depletion is particularly relevant given its role in detoxifying lipid hydroperoxides and protecting membrane integrity [38,39], as its loss may sensitize hepatocytes to oxidative membrane damage and ferroptosis, a cell death modality increasingly implicated in metabolic liver disease progression. Superoxide dismutase 1 (SOD1) levels declined progressively in both BSA and FA conditions at 28 d (Figure 4E, F), suggesting a time-dependent erosion of superoxide detoxification capacity that operates partly independently of lipid treatment, and that may be further compounded by chronic lipotoxic stress [40].

In parallel with the collapse of antioxidant defenses, chronic lipid stress fundamentally reshaped ER stress and autophagic responses. The unfolded protein response displayed a biphasic trajectory: PERK expression was elevated during acute exposure, consistent with early adaptive UPR activation to restore ER proteostasis, but became markedly suppressed after prolonged treatment (Figure 4G, H). Spliced XBP1 (XBP1s) was significantly increased at day 28 (Figure 4G, H). This pattern suggests a shift from coordinated, multibranch UPR activation toward

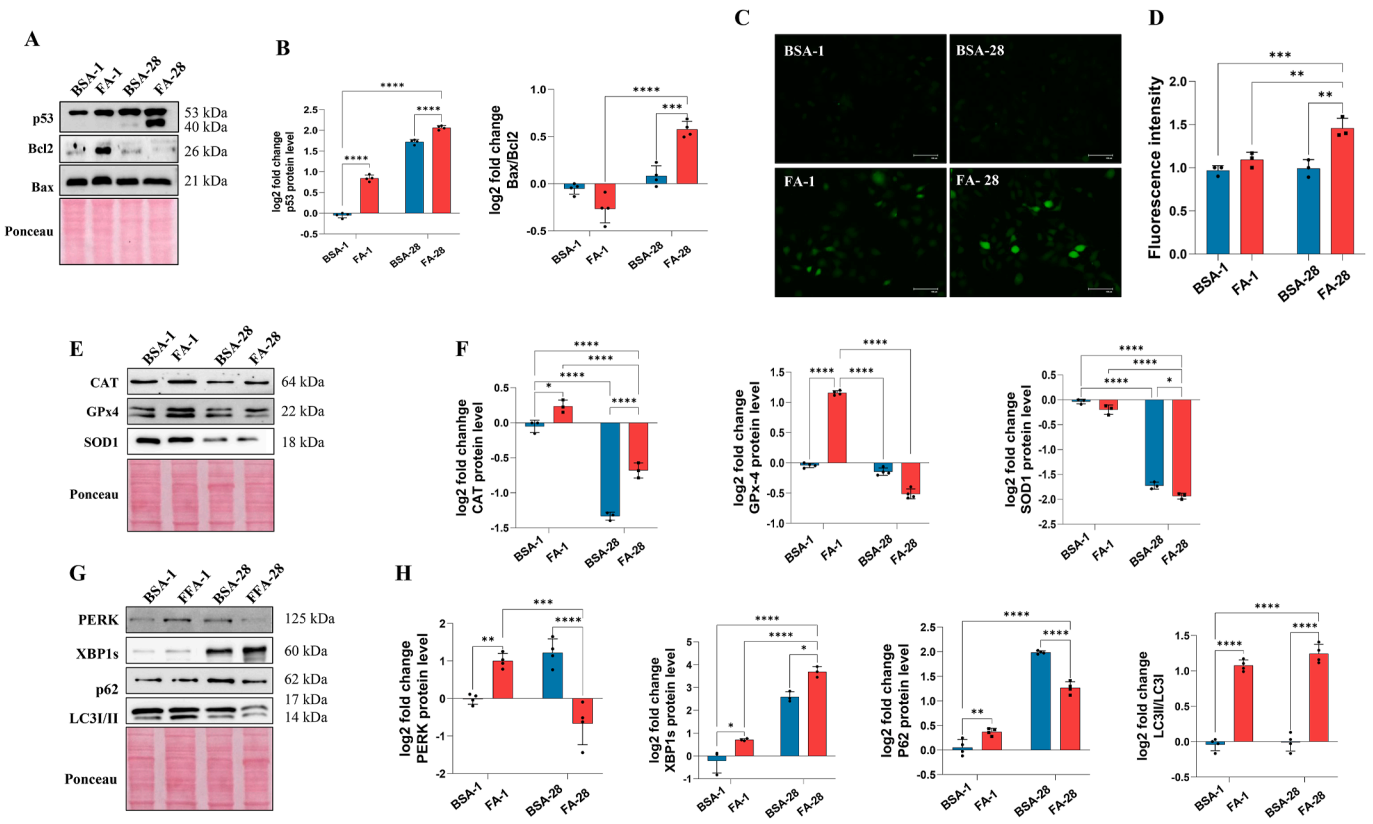

FIGURE 4. Fatty acid (FA)-induced oxidative stress and cellular stress responses in HuH7 cells. (A) Representative Western blot analysis of P53, Bcl-2, and Bax protein levels, (B) Bax/Bcl-2 ratio, and P53 relative densitometric quantification in HuH7 cells treated with BSA or FA at day 1 and day 28. (C) Representative fluorescence microscopy images of intracellular reactive oxygen species (ROS) detected by DCFH-DA staining in HuH7 cells treated with Vehicle (BSA) or FAs (PA/OA 1:1) for 1 d and 28 d. Scale bar = 100 μm. (D) Quantification of ROS based on mean fluorescence intensity analysis using ImageJ software, normalized to the BSA-1 control group. (E) Representative Western blot analysis of antioxidant enzymes catalase (CAT), glutathione peroxidase-4 (GPx-4), and superoxide dismutase 1 (SOD1), with (F) relative densitometric quantification in HuH7 cells treated with BSA or FA at day 1 and day 28. (G) Western blot analysis of ER stress and autophagy markers PERK, XBP1s, p62, LC3I, and LC3II, with (H) quantification of PERK, XBP1s, p62, and LC3II/LC3I ratio in HuH7 cells under the indicated conditions. Data are presented as mean ± SEM from 3 independent experiments. Quantitative data are expressed as fold change relative to BSA-1 or log2 fold change relative to BSA-1. Statistical significance: $^{*}P < 0.05$; $^{**}P < 0.01$; $^{***}P < 0.005$; $^{****}P < 0.001$. Bax, BCL2-associated X protein; Bcl-2, B-cell lymphoma 2; BSA, bovine serum albumin; DCFH-DA, 2',7'-dichlorodihydrofluorescein diacetate; LC3I/II, Microtubule-associated protein light chain 3 I/II; OA, oleic acid; PA, palmitic acid; PERK, Protein Kinase R-like Endoplasmic Reticulum Kinase; XBP1s, X-box binding protein 1.

selective and sustained IRE1/XBP1s engagement, a configuration associated with maladaptive ER stress signaling in the context of chronic metabolic disease.

Autophagic activity, by contrast, remained sustained throughout both phases. Increased LC3II/LC3I ratios and reduced p62 levels at both time points (Figure 4G, H) indicate enhanced autophagic flux rather than pathway blockage, suggesting that lipophagy and general autophagy remain functionally intact and may serve as a salvage mechanism to clear damaged organelles and LDs under chronic stress. However, the persistence of autophagic activity was insufficient to prevent oxidative damage accumulation and cell death, indicating that autophagy alone cannot compensate for the broader failure of redox and proteostatic control.

Effect of acute and chronic FA exposure on insulin receptor and AKT signaling in hepatocytes

To investigate whether lipotoxicity induces changes in insulin responsiveness in hepatocytes, we analyzed total and phosphorylated insulin receptor (IR) and AKT protein levels following an acute insulin stimulation step immediately before cell lysis [18].

At 1 d, total IR and total AKT protein levels were comparable between BSA- and FA-treated cells, indicating that short-term FA exposure did not affect protein expression (Figure 5A–C). Insulin stimulation increased IR and AKT phosphorylation in both experimental conditions. Although FA-treated cells showed a mild reduction in insulin-stimulated AKT phosphorylation compared with controls, the insulin response was largely preserved, as reflected by the maintained pAKT/AKT ratio (Figure 5A–C).

At 28 d, total IR and AKT levels remained largely unchanged between BSA and FA conditions. However, insulin-stimulated phosphorylation of both IR and AKT was markedly reduced in FA-treated cells compared with controls. AKT phosphorylation in response to insulin was strongly blunted after chronic FA exposure, resulting in a significant decrease in the pAKT/AKT ratio despite the presence of insulin (Figure 5A–C).

Overall, these results indicate that acute FA exposure induces only a modest impairment of insulin signaling, whereas chronic FA treatment leads to a pronounced defect in insulin-stimulated

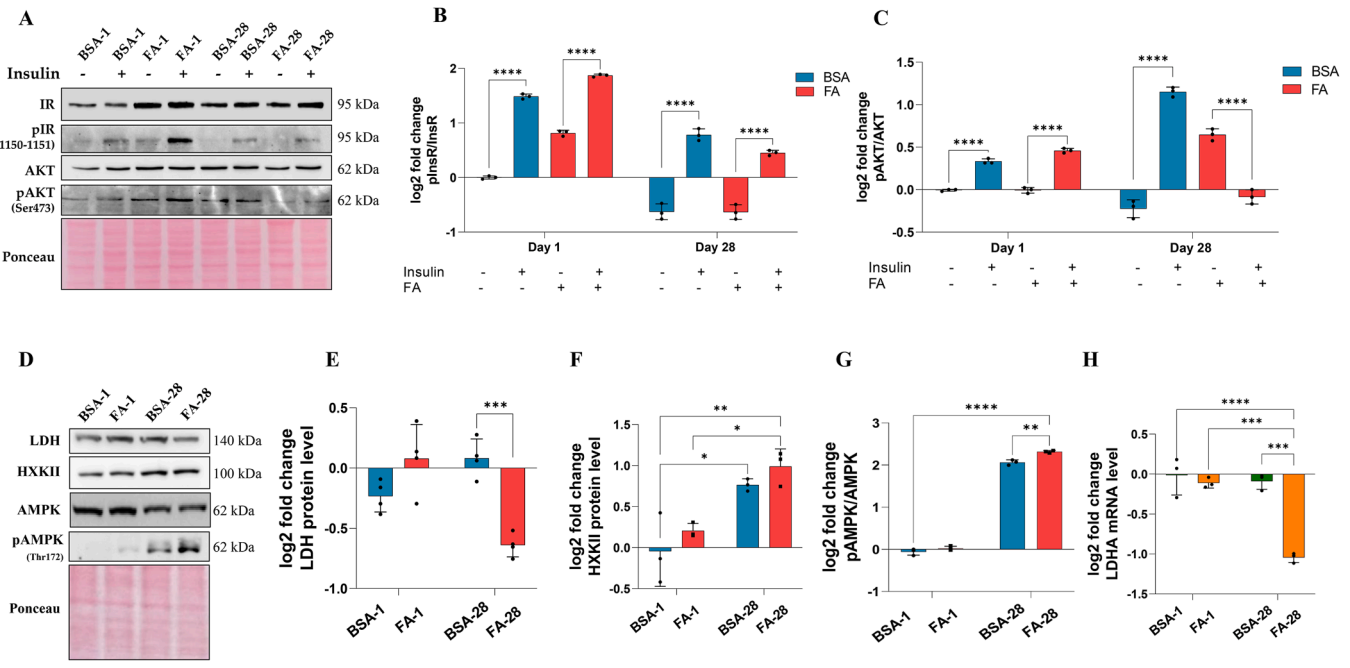

FIGURE 5. Long-term fatty acid (FA) exposure impairs cellular bioenergetic homeostasis. (A) Representative Western blot analysis of insulin pathway markers insulin receptor (IR), pIR (Tyr1150-1151), AKT, and pAKT (Ser473), with (B, C) pIR/IR and pAKT/AKT ratio in HuH7 cells treated with BSA or FA at day 1 and day 28, followed by acute stimulation with 100 nM insulin for 10 min immediately before lysis. (D) Representative Western blot analysis of bioenergetic markers lactate dehydrogenase (LDH), hexokinase II (HKII), AMPK, and phospho-AMPK (Thr172), with (E, F) relative quantification. (G) pAMPK/AMPK ratio in HuH7 cells treated with BSA or FA at day 1 and day 28. (H) Relative mRNA expression levels of LDHA. Data are presented as mean ± SEM from 3 independent experiments. Quantitative data are shown as log2 fold change relative to BSA-1. Statistical significance: $^{*}P < 0.05$; $^{**}P < 0.01$; $^{***}P < 0.005$; $^{****}P < 0.001$. AKT, Protein Kinase B; AMPK, AMP-activated protein kinase; BSA, bovine serum albumin; LDHA, L-lactate dehydrogenase A.

AKT activation, consistent with the development of insulin resistance at later time points.

The expression of hexokinase II (HKII) increased while that of lactate dehydrogenase strongly decreased, both at the level of protein and mRNA (Figure 5D–F,H). The metabolic shift toward oxidative metabolism throughout prolonged lipid exposure was paralleled by activation of AMPK (Figure 5D, G), a hallmark of energetic stress and master regulator of catabolic metabolism.

Consistent with these results, immunoblot analysis revealed that acute exposure to FA induced a significant increase in the protein levels of multiple mitochondrial respiratory complexes, including complex V (ATP5A), complex III (UQCRC2), complex II (SDHB), and complex I (NDUFB8), compared with BSA-treated controls (Figure 6A–E). After prolonged lipid exposure (28 d), expression of these mitochondrial complexes remained elevated or further increased, with complex II showing the most pronounced and consistent upregulation relative to both acute treatment and time-matched controls (Figure 6A–E), consistent with adaptations to accommodate elevated β-oxidation flux and maintain ATP production under metabolic stress.

Chronic lipid exposure alters mitochondrial and SIRT1/CLOCK-associated regulatory markers

In contrast to the sustained increase in mitochondrial respiratory complex expression, prolonged FA exposure was associated with a significant reduction in SIRT1 protein levels (Figure 6F, G). To interpret mitochondrial and regulatory adaptations in the context of chronic FA exposure, it is important to note that these experiments were performed in low-glucose medium without insulin supplementation. Thus, cells were not exposed to sustained high-glucose/high-insulin conditions during the 28-d treatment period. SIRT1 is a NAD^{+}-dependent deacetylase that plays a pivotal role in coordinating mitochondrial function, FAO, antioxidant defenses, autophagy, and ER stress resolution through deacetylation of key transcriptional regulators, including components of the circadian clock machinery. Its downregulation under chronic lipid stress likely reflects a state of persistent energetic and redox imbalance, potentially driven by NAD^{+} depletion secondary to sustained β-oxidation.

Notably, prolonged lipid exposure was associated with a progressive decline in SIRT1 expression (Figure 6F, G). In parallel, chronic lipid overload was associated with a marked suppression of CLOCK protein expression (Figure 6F, H), indicating disruption of the hepatocyte circadian machinery. Importantly, the decline in both SIRT1 and CLOCK was specific to prolonged lipid exposure, as time-matched BSA-treated controls displayed only moderate reductions. Together, these results indicate that chronic lipid overload is associated with sustained upregulation of mitochondrial respiratory complexes alongside a concomitant

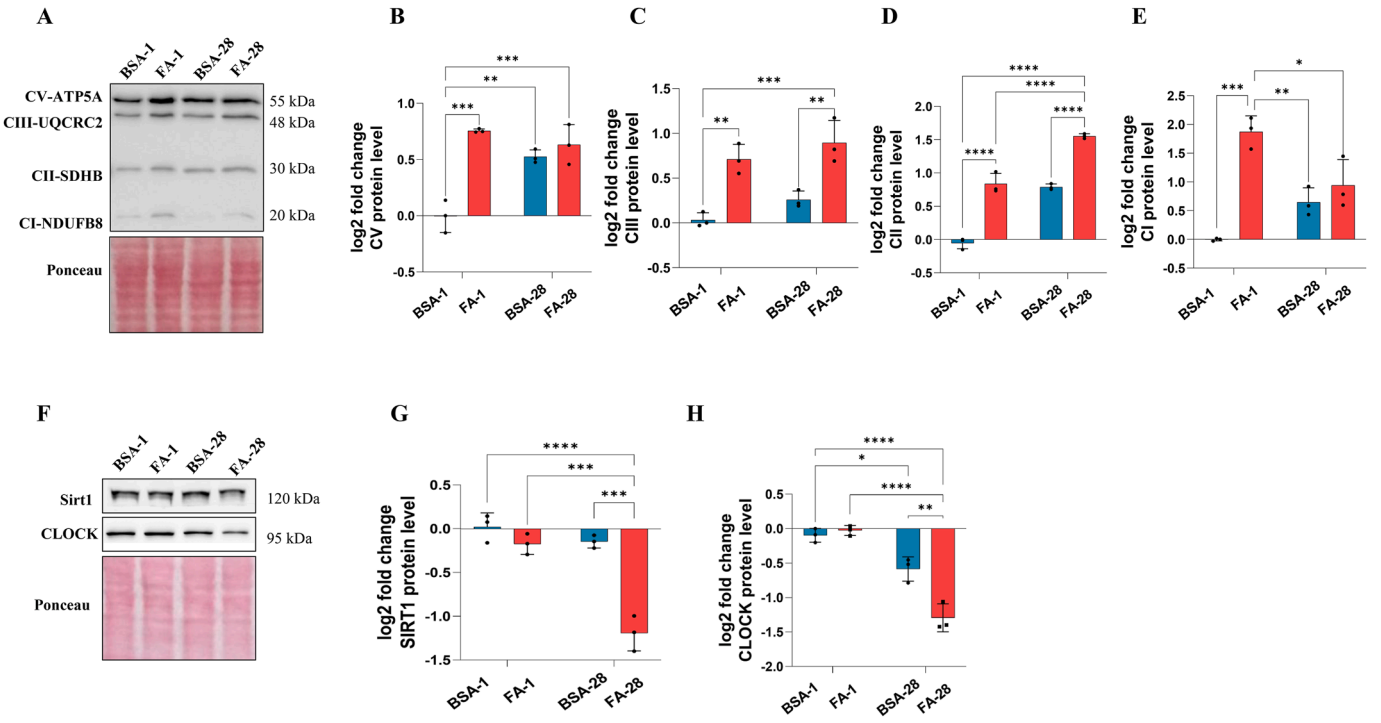

FIGURE 6. Extended fatty acid (FA) treatment compromises mitochondrial complex and alters circadian clock regulators. (A) Western blot analysis of mitochondrial respiratory chain complexes, with (B–E) relative densitometric quantification. (F) Western blot analysis of SIRT1 and CLOCK protein levels, with (G, H) relative quantification in HuH7 cells treated with BSA or FA at day 1 and day 28. Data are presented as mean ± SEM from 3 independent experiments. Quantitative data are shown as log2 fold change relative to BSA-1. Statistical significance: $^{*}P < 0.05$; $^{**}P < 0.01$; $^{***}P < 0.005$; $^{****}P < 0.001$. BSA, bovine serum albumin; CV-ATP5A, complex V, ATP synthase subunit alpha; CI-NDUFB8, complex I, NADH:ubiquinone oxidoreductase subunit B8; CII-SDHB, complex II, succinate dehydrogenase iron-sulfur subunit; CLOCK, Circadian Locomotor Output Cycles Kaput; SIRT1, sirtuin 1.

reduction in SIRT1 and CLOCK protein expression, revealing a divergence between mitochondrial expansion and higher-level metabolic and circadian regulatory pathways during prolonged lipotoxic stress.

Discussion

The present study provides a temporal characterization of the hepatocellular response to sustained FA overload and identifies the progressive loss of regulatory coordination as a key event underlying the transition from metabolic adaptation to cellular dysfunction. By comparing acute and prolonged exposure to a PA/OA mixture, we show that hepatocytes initially activate effective protective mechanisms that preserve metabolic homeostasis, whereas chronic lipid exposure progressively uncouples these adaptive responses, ultimately resulting in oxidative stress, insulin resistance, and cell death. These findings support the concept that lipotoxicity arises not simply from lipid accumulation per se but from the inability to sustain long-term integration among metabolic, redox, and stress-response pathways.

During the early phase of exposure (day 1), hepatocytes efficiently buffered FA overload through enhanced neutral lipid storage. Because BODIPY 493/503 specifically labels intracellular neutral lipids, the sustained accumulation of LDs throughout the experiment reflects the dynamic balance among FA uptake, esterification, storage, mobilization, and oxidation rather than FA uptake alone [41,42]. The marked increase in LD content together with DGAT1 induction is consistent with the established cytoprotective role of triacylglycerol synthesis and LD biogenesis in preventing the accumulation of toxic lipid intermediates [43]. At this stage, cell viability, morphology, apoptotic markers, and insulin responsiveness remained largely preserved, whereas increased catalase and GPx-4 expression indicated activation of an adaptive antioxidant response. Exometabolomic analysis further supported an early adaptive phenotype, revealing higher residual glucose together with lower pyruvate, lactate, acetate, and glutamine levels compared with controls. These findings suggest preferential utilization of exogenous FA as an energy source, limiting glycolytic engagement and amino acid catabolism. The preservation of FASN and ACC expression further indicates that hepatocytes retained substantial metabolic flexibility during this initial phase, consistent with previous models of early steatotic adaptation [44].

A distinct metabolic phenotype emerged after 14 d of treatment. Although cell viability and lipid storage capacity were still largely preserved, exometabolomic profiling revealed marked remodeling of carbon and amino acid metabolism, characterized by increased lactate and alanine levels together with enhanced glutamine consumption. The pronounced lactate accumulation in the medium, the highest observed across all conditions, suggests increased glycolytic flux and reflects an energetic demand that could no longer be fully sustained by oxidative metabolism alone. Consistent with this interpretation, FASN and ACC

protein levels were significantly reduced, indicating diversion of carbon substrates away from de novo lipogenesis toward energy-producing pathways. Elevated alanine levels may reflect impaired hepatic alanine disposal, a phenomenon previously associated with hepatic steatosis and reduced glucagon-dependent amino acid catabolism [45]. Indeed, hepatic steatosis has been shown to reduce glucagon receptor abundance, thereby attenuating downstream signaling involved in alanine transport and metabolism [46].

Concurrently, lower extracellular pyruvate levels suggest increased intracellular pyruvate utilization either for lactate production or mitochondrial oxidation. The induction of CPT1A in the absence of a significant decline in SIRT1 further indicates that mitochondrial oxidative capacity remained functional at this stage. Collectively, these findings identify day 14 as a transitional phase in which metabolic compensation is still maintained but increasingly relies on the coordinated engagement of glycolytic, amino acid, and oxidative pathways, indicating that hepatocytes are approaching the limits of their adaptive capacity before overt cytotoxicity becomes evident.

This adaptive state was not maintained during prolonged exposure. At day 28, FA treatment resulted in progressive ROS accumulation accompanied by a marked reduction in antioxidant defenses. The decline in catalase, GPx-4, and SOD1 expression indicates a reduced capacity to neutralize ROS, thereby promoting a pro-oxidant intracellular environment. Particularly relevant is the depletion of GPx-4, a key regulator of lipid peroxide detoxification and membrane protection [47], whose loss has been linked to increased susceptibility to ferroptosis and lipotoxic injury in metabolic liver disease. In parallel, chronic FA exposure induced profound impairment of insulin signaling, as demonstrated by reduced insulin-stimulated AKT activation despite preserved insulin receptor expression, suggesting that chronic lipotoxicity primarily affects postreceptor signaling events [48–50].

The deterioration of redox homeostasis was accompanied by activation of cell death pathways. Chronic treatment shifted the balance of Bcl2 family proteins toward apoptosis, as evidenced by the marked increase in the Bax/Bcl2 ratio. These alterations were associated with sustained p53 accumulation and progressive cell loss. Given the established role of p53 as an integrator of metabolic, oxidative, and genotoxic stress signals [51], its induction likely reflects the inability of hepatocytes to resolve chronic metabolic stress. Although the molecular identity of the p53 doublet remains unclear, stress-induced p53 processing has previously been associated with the generation of mitochondrial-localized forms capable of amplifying apoptotic signaling [52].

The metabolic phenotype observed at day 28 further supports the concept of adaptive failure rather than successful metabolic reprogramming. Hepatocytes responded to prolonged FA excess by suppressing lipogenic enzymes and reducing FA uptake capacity, as indicated by the downregulation of FASN, ACC, CD36, and FABP1. Conversely, CPT1A expression, AMPK activation, and increased abundance of mitochondrial respiratory chain complexes were consistent with an attempt to sustain FAO and mitochondrial energy production [53]. Importantly, these molecular changes should be interpreted as indicators of enhanced oxidative capacity rather than direct evidence of increased β-oxidation flux, which was not measured in the present study. Reduced net palmitate accumulation, together with the downregulation of CD36 and FABP1, further supports altered FA handling during chronic exposure. However, the present assay does not allow discrimination between reduced FA uptake and changes in intracellular retention, efflux, or metabolic partitioning. Clarifying the relative contribution of these mechanisms will require dedicated studies.

Exometabolomic data provide additional insight into the metabolic consequences of this chronic response. The increase in residual glucose, accompanied by lower lactate levels relative to day 14, suggests reduced glycolytic output despite increased HKII expression. Under these conditions, glucose-derived carbon may be redirected toward pathways such as the pentose phosphate pathway rather than lactate production or de novo lipogenesis, which is unlikely given the marked suppression of SREBP-1, FASN, and ACC activity. Such metabolic rerouting could provide NADPH to sustain antioxidant defenses and support nucleotide synthesis and protein glycosylation during persistent cellular stress. In addition, the progressive accumulation of extracellular acetate throughout the experimental period deserves particular attention. Hepatic acetate may originate from acetyl-CoA hydrolysis, incomplete FAO, or alternative acetyl-CoA disposal pathways [54,55]. The sustained increase in acetate secretion, occurring alongside CPT1A induction and enhanced respiratory complex abundance, may therefore reflect acetyl-CoA overflow resulting from FAO rates exceeding tricarboxylic acid cycle capacity. Alternatively, it may indicate impaired channeling of acetyl-CoA into downstream anabolic pathways as lipogenesis becomes progressively suppressed. In either case, acetate accumulation provides an independent readout of the metabolic imbalance between FAO and acetyl-CoA utilization that characterizes the chronic stage of lipid overload.

A central mechanistic insight emerging from this study is the progressive decline of SIRT1 and CLOCK expression during chronic FA exposure. SIRT1 is a critical regulator linking nutrient sensing, mitochondrial function, antioxidant defenses, autophagy, and ER stress responses through NAD^+-dependent signaling [56], whereas CLOCK coordinates circadian regulation of hepatic metabolism and energy homeostasis [57–59]. The concomitant reduction of these regulators occurred despite persistent AMPK activation and increased abundance of mitochondrial respiratory complexes, indicating that hepatocytes retain the ability to activate compensatory metabolic programs but progressively lose the higher-order regulatory networks required to coordinate them efficiently. Consistent with this interpretation, acute FA exposure induced PERK expression, suggesting activation of a protective unfolded protein response, whereas chronic treatment resulted in PERK suppression and persistent activation of the XBP1s branch, indicative of dysregulated ER stress signaling [60–63]. Although autophagic activity appeared to remain active throughout the experimental period, as indicated by increased LC3II/LC3I ratios and reduced p62 abundance, maintenance of autophagic flux alone was insufficient to prevent oxidative damage and cell death. Together, these findings suggest that chronic lipotoxicity is characterized not by the failure of a single adaptive pathway but by the progressive loss of regulatory coordination among multiple stress-response systems.

Several limitations should be acknowledged. The study did not directly quantify intracellular lipid species, β-oxidation rates, or mitochondrial function. Consequently, the molecular changes reported here should be interpreted as indicators of metabolic remodeling rather than direct measurements of pathway activity. In addition, the PA/OA mixture reproduces only part of the complexity of the circulating FA environment and therefore represents a reductionist model of lipid overload. Nevertheless, the prolonged exposure paradigm employed in this study provides a valuable framework for investigating the temporal dynamics of lipotoxic adaptation and failure that are not captured by conventional short-term models.

In conclusions, overall, our data support a temporal organization of the response, suggesting a 3-stage process. An initial adaptive phase (day 1) is followed by a compensatory remodeling phase (day 14), characterized by extensive metabolic reorganization in the absence of overt cellular dysfunction, and finally by a decompensated phase (day 28), in which persistent oxidative stress, impaired signaling, and loss of regulatory coordination culminate in cell death. This intermediate compensatory stage may be particularly relevant to MASLD progression because it likely corresponds to the period during which hepatocytes remain functionally viable despite increasing metabolic stress and therefore may represent a critical therapeutic window. In this context, preservation of redox balance, NAD^+ homeostasis, and SIRT1/CLOCK-dependent signaling may represent key targets for maintaining hepatocyte resilience during chronic lipid overload and for limiting the transition from adaptive steatosis to progressive metabolic liver disease.

Author contributions

The authors' responsibilities were as follows – IS, AMG: contributed to conceptualization; IS, EB, FV, AMG: contributed to data curation; IS, EB, ES, DV, FA, FDC: contributed to formal analysis; AMG: contributed to funding acquisition, investigation, supervision, and validation; IS, EB, FV, ES: contributed to methodology; EB, FV, FPF: contribute to resources and software; IS, AMG: contributed to writing – original draft; IS, EB, FV, ES, DV: contributed to writing – review and editing; and all authors: read and approved the final manuscript.

Declaration of generative AI and AI-assisted technologies in the writing process

The author(s) declare that no generative AI or AI-assisted technologies were used in the writing of this manuscript.

Conflict of interest

The authors report no conflicts of interest.

Funding

We acknowledge support from the *IDENTITA* project (T5-AN-01), "Integrated Mediterranean Network for Personalized Nutrition Pathways against Malnutrition," coordinated by the Puglia Region—Health Marketplace.

Appendix A. Supplementary data

Supplementary data to this article can be found online at https://doi.org/10.1016/j.tjnut.2026.101774.

References

[1] L. Hodson, P.J. Gunn, The regulation of hepatic fatty acid synthesis and partitioning: the effect of nutritional state, Nat. Rev. Endocrinol. 15 (12) (2019) 689–700, https://doi.org/10.1038/s41574-019-0256-9.
[2] H. Tilg, T.E. Adolph, M. Dudek, P. Knolle, Non-alcoholic fatty liver disease: the interplay between metabolism, microbes and immunity, Nat. Metab. 3 (12) (2021) 1596–1607, https://doi.org/10.1038/s42255-021-00501-9.
[3] H. Tilg, S. Petta, N. Stefan, G. Targher, Metabolic dysfunction–associated steatotic liver disease in adults, JAMA. 335 (2) (2026) 163, https://doi.org/10.1001/jama.2025.19615.
[4] D. Misceo, G. Mocciaro, S. D'Amore, M. Vacca, Diverting hepatic lipid fluxes with lifestyles revision and pharmacological interventions as a strategy to tackle steatotic liver disease (SLD) and hepatocellular carcinoma (HCC), Nutr. Metab. 21 (1) (2024) 112, https://doi.org/10.1186/s12986-024-00871-3.
[5] Y. Wei, D. Wang, F. Topczewski, M.J. Pagliassotti, Saturated fatty acids induce endoplasmic reticulum stress and apoptosis independently of ceramide in liver cells, Am. J. Physiol. Endocrinol. Metab. 291 (2) (2006) E275–E281, https://doi.org/10.1152/ajpendo.00644.2005.
[6] C. Moliterni, F. Vari, E. Schifano, S. Tacconi, E. Stanca, M. Friuli, et al., Lipotoxicity of palmitic acid is associated with DGAT1 downregulation and abolished by PPARα activation in liver cells, J. Lipid, Res 65 (12) (2024) 100692, https://doi.org/10.1016/j.jlr.2024.100692.
[7] J.N. Falcone, M.A. Hurd, S. Kumar, M. Yeung, C. Newberry, M.Y. So, et al., The ratio of unsaturated to saturated fatty acids is a distinguishing feature of NAFLD in subjects with metabolic disease, J. Endocr. Soc. 5 (Suppl 1) (2021), https://doi.org/10.1210/jendso/bvab048.859. A421–A421.
[8] H. Malhi, G. Gores, Molecular mechanisms of lipotoxicity in nonalcoholic fatty liver disease, Semin. Liver Dis. 28 (4) (2008) 360–369, https://doi.org/10.1055/s-0028-1091980.
[9] X. Zeng, M. Zhu, X. Liu, X. Chen, Y. Yuan, L. Li, et al., Oleic acid ameliorates palmitic acid induced hepatocellular lipotoxicity by inhibition of ER stress and pyroptosis, Nutr. Metab. 17 (1) (2020) 11, https://doi.org/10.1186/s12986-020-0434-8.
[10] X. Li, J. Zhang, S. Luo, X. Yu, C. Song, Crosstalk between lipid droplets and autophagy in cancer: a nexus for therapeutic targeting, Pharmacol. Res. 222 (2025) 108023, https://doi.org/10.1016/j.phrs.2025.108023.
[11] L. Bideyan, R. Nagari, P. Tontonoz, Hepatic transcriptional responses to fasting and feeding, Genes Dev 35 (9-10) (2021) 635–657, https://doi.org/10.1101/gad.348340.121.
[12] C.N. Tzouanas, J.E.S. Shay, M.S. Sherman, A.J. Rubin, B.E. Mead, T. T. Dao, et al., Hepatic adaptation to chronic metabolic stress primes tumorigenesis, Cell 189 (2) (2026) 435–460.e28, https://doi.org/10.1016/j.cell.2025.11.031.
[13] Y. Liu, Y. Wang, J. Zhou, H. Li, C. Liu, B. Zhong, et al., Restoring metabolic flexibility: targeting organelle interaction networks in the pathogenesis and therapy of MASLD, Front. Cell Dev. Biol. 13 (2025) 1718799, https://doi.org/10.3389/fcell.2025.1718799.
[14] H.-Y. Liu, C.-F. Chang, C.-C. Lu, S.-C. Wu, B. Huang, T.-L. Cheng, et al., The role of mitochondrial metabolism, AMPK-SIRT mediated pathway, LncRNA and MicroRNA in osteoarthritis, Biomedicines 10 (7) (2022) 1477, https://doi.org/10.3390/biomedicines10071477.
[15] Y. Olmos, F.J. Sánchez-Gómez, B. Wild, N. García-Quintans, S. Cabezudo, S. Lamas, et al., SirT1 regulation of antioxidant genes is dependent on the formation of a FoxO3a/PGC-1α complex, Antioxid. Redox. Signal. 19 (13) (2013) 1507–1521, https://doi.org/10.1089/ars.2012.4713.
[16] C. Cantó, L.Q. Jiang, A.S. Deshmukh, C. Mataki, A. Coste, M. Lagouge, et al., Interdependence of AMPK and SIRT1 for metabolic adaptation to fasting and exercise in skeletal muscle, Cell, Metab 11 (3) (2010) 213–219, https://doi.org/10.1016/j.cmet.2010.02.006.
[17] N. Alsabeeh, B. Chausse, P.A. Kakimoto, A.J. Kowaltowski, O. Shirihai, Cell culture models of fatty acid overload: Problems and solutions, Biochim. Biophys. Acta Mol. Cell Biol. Lipids. 1863 (1) (2018) 143–151, https://doi.org/10.1016/j.bbalip.2017.11.006.
[18] S. Tacconi, F. Vari, C. Sbarigia, D. Vardanyan, S. Longo, F. Mura, et al., M1-derived extracellular vesicles polarize recipient macrophages into M2-like macrophages and alter skeletal muscle homeostasis in a hyperglucose environment, Cell. Commun. Signal. 22 (1) (2024) 193, https://doi.org/10.1101/2023.10.03.560690.

[19] M. Ricchi, M.R. Odoardi, L. Carulli, C. Anzivino, S. Ballestri, A. Pinetti, et al., Differential effect of oleic and palmitic acid on lipid accumulation and apoptosis in cultured hepatocytes, J. Gastroenterol. Hepatol. 24 (5) (2009) 830–840, https://doi.org/10.1111/j.1440-1746.2008.05733.x.
[20] M. Lepretti, S. Martucciello, M.A. Burgos Aceves, R. Putti, L. Lionetti, Omega-3 fatty acids and insulin resistance: focus on the regulation of mitochondria and endoplasmic reticulum stress, Nutrients 10 (3) (2018) 350, https://doi.org/10.3390/nu10030350.
[21] A. Moravcová, Z. Červinková, O. Kučera, V. Mezera, D. Rychtrmoc, H. Lotková, The effect of oleic and palmitic acid on induction of steatosis and cytotoxicity on rat hepatocytes in primary culture, Physiol. Res. 64 (Suppl 5) (2015) S627–S636, https://doi.org/10.33549/physiolres.933224.
[22] X. Chen, L. Li, X. Liu, R. Luo, G. Liao, L Li, et al., Oleic acid protects saturated fatty acid mediated lipotoxicity in hepatocytes and rat of non-alcoholic steatohepatitis, Life. Sci. 203 (2018) 291–304, https://doi.org/10.1016/j.lfs.2018.04.022.
[23] M.J. Gómez-Lechón, M.T. Donato, A. Martínez-Romero, N. Jiménez, J. V. Castell, J.E. O'Connor, A human hepatocellular in vitro model to investigate steatosis, Chem. Biol. Interact. 165 (2) (2007) 106–116, https://doi.org/10.1016/j.cbi.2006.11.004.
[24] S. Kamiloglu, G. Sari, T. Ozdal, E. Capanoglu, Guidelines for cell viability assays, Food Front 1 (3) (2020) 332–349, https://doi.org/10.1002/fft2.44.
[25] W. Stremmel, P.D. Berk, Hepatocellular influx of [14C]oleate reflects membrane transport rather than intracellular metabolism or binding, Proc. Natl Acad. Sci. U.S.A. 83 (10) (1986) 3086–3090, https://doi.org/10.1073/pnas.83.10.3086.
[26] F. De Castro, M. Benedetti, G. Antonaci, L. Del Coco, S.A. De Pascali, A. Muscella, et al., Response of cisplatin resistant Skov-3 cells to [Pt(O, O'-Acac)(γ-Acac)(DMS)] treatment revealed by a metabolomic ^{1}H-NMR study, Molecules 23 (9) (2018) 2301, https://doi.org/10.3390/molecules23092301.
[27] F. De Castro, E. Stefàno, E. De Luca, A. Muscella, S. Marsigliante, M. Benedetti, et al., A NMR-based metabolomic approach to investigate the antitumor effects of the novel [Pt(η1-C2H4OMe)(DMSO)(phen)]+ (phen = 1,10-Phenanthroline) compound on neuroblastoma cancer cells, Bioinorg. Chem. Appl. 2022 (1) (2022) 8932137, https://doi.org/10.1155/2022/8932137.
[28] T. Fan, Metabolite profiling by one- and two-dimensional NMR analysis of complex mixtures, Prog. Nucl. Magn. Reson. Spectrosc. 28 (1998) 161–219, https://doi.org/10.1016/0079-6565(96)90002-3.
[29] R. Bro, K. Kjeldahl, A.K. Smilde, H.A. Kiers, Cross-validation of component models: a critical look at current methods, Anal. Bioanal. Chem. 390 (5) (2008) 1241–1251, https://doi.org/10.1007/s00216-007-1790-1.
[30] J. Feng, J. Li, H. Wu, Z. Chen, Metabolic responses of HeLa cells to silica nanoparticles by NMR-based metabolomic analyses, Metabolomics 9 (4) (2013) 874–886, https://doi.org/10.1007/s11306-013-0499-8.
[31] A.E. Feldstein, N.W. Werneburg, Z. Li, S.F. Bronk, G.J. Gores, Bax inhibition protects against free fatty acid-induced lysosomal permeabilization, Am. J. Physiol. Gastrointest. Liver Physiol. 290 (6) (2006) G1339–G1346, https://doi.org/10.1152/ajpgi.00509.2005.
[32] H.-P. Zhao, Y.-R. Xie, Expression of Bcl-2 and Bax in hepatocytes in nonalcoholic fatty liver disease, World Chin. J. Digestol. 17 (23) (2009) 2409, https://doi.org/10.11569/wcjd.v17.i23.2409.
[33] T. Ozaki, A. Nakagawara, Role of p53 in cell death and human cancers, Cancers (Basel) 3 (1) (2011) 994–1013, https://doi.org/10.3390/cancers3010994.
[34] K.Y. Koo, K. Moon, H.S. Song, M.-S. Lee, Metabolic regulation by p53: implications for cancer therapy, Mol. Cells. 48 (4) (2025) 100198, https://doi.org/10.1016/j.mocell.2025.100198.
[35] J.-F. Millau, O.J. Bandele, J. Perron, N. Bastien, É.F. Bouchard, L. Gaudreau, et al., Formation of stress-specific p53 binding patterns is influenced by chromatin but not by modulation of p53 binding affinity to response elements, Nucleic Acids Res 39 (8) (2011) 3053–3063, https://doi.org/10.1093/nar/gkq1209.
[36] T. Kuilman, D.S. Peeper, Senescence-messaging secretome: SMS-ing cellular stress, Nat. Rev. Cancer. 9 (2) (2009) 81–94, https://doi.org/10.1038/nrc2560.
[37] R. Chiarle, Y. Zhang, R.L. Frock, S.M. Lewis, B. Molinie, Y.-J. Ho, et al., Genome-wide translocation sequencing reveals mechanisms of chromosome breaks and rearrangements in B cells, Cell 147 (1) (2011) 107–119, https://doi.org/10.1016/j.cell.2011.07.049.
[38] J. Qi, J.-W. Kim, Z. Zhou, C.-W. Lim, B. Kim, Ferroptosis affects the progression of nonalcoholic steatohepatitis via the modulation of lipid peroxidation–mediated cell death in mice, Am. J. Pathol. 190 (1) (2020) 68–81, https://doi.org/10.1016/j.ajpath.2019.09.011.
[39] S. Tsurusaki, Y. Tsuchiya, T. Koumura, M. Nakasone, T. Sakamoto, M. Matsuoka, et al., Hepatic ferroptosis plays an important role as the trigger for initiating inflammation in nonalcoholic steatohepatitis, Cell. Death Dis. 10 (6) (2019) 449, https://doi.org/10.1038/s41419-019-1678-y.
[40] S. Wang, Z. Liu, J. Geng, L. Li, X. Feng, An overview of ferroptosis in non-alcoholic fatty liver disease, Biomed. Pharmacother. 153 (2022) 113374, https://doi.org/10.1016/j.biopha.2022.113374.
[41] B. Qiu, M.C. Simon, BODIPY 493/503 staining of neutral lipid droplets for microscopy and quantification by flow cytometry, Bio. Protoc. 6 (17) (2016) e1912, https://doi.org/10.21769/bioprotoc.1912.
[42] J.A. Olzmann, P. Carvalho, Dynamics and functions of lipid droplets, Nat. Rev. Mol. Cell. Biol. 20 (3) (2019) 137–155, https://doi.org/10.1038/s41580-018-0085-z.
[43] E. Obaseki, D. Adebayo, S. Bandyopadhyay, H. Hariri, Lipid droplets and fatty acid-induced lipotoxicity: in a nutshell, FEBS Lett 598 (10) (2024) 1207–1214, https://doi.org/10.1002/1873-3468.14808.
[44] A. Allameh, R. Niayesh-Mehr, A. Aliarab, G. Sebastiani, K. Pantopoulos, Oxidative stress in liver pathophysiology and disease, Antioxidants 12 (9) (2023) 1653, https://doi.org/10.3390/antiox12091653.
[45] M. Winther-Sørensen, K.D. Galsgaard, A. Santos, S.A.J. Trammell, K. Sulek, R.E. Kuhre, J. Pedersen, et al., Glucagon acutely regulates hepatic amino acid catabolism and the effect may be disturbed by steatosis, Mol. Metab. 42 (2020) 101080, https://doi.org/10.1016/j.molmet.2020.101080.
[46] A. Charbonneau, C.G. Unson, J.M. Lavoie, High-fat diet-induced hepatic steatosis reduces glucagon receptor content in rat hepatocytes: potential interaction with acute exercise, J. Physiol. 579 (Pt 1) (2007) 255–267, https://doi.org/10.1113/jphysiol.2006.121954.
[47] M. Maiorino, M. Conrad, F. Ursini, GPx4, lipid peroxidation, and cell death: discoveries, rediscoveries, and open issues, Antioxid. Redox. Signal. 29 (1) (2018) 61–74, https://doi.org/10.1089/ars.2017.7115.
[48] M. Olivares-Vicente, M. Herranz-López, The interplay between oxidative stress and lipid composition in obesity-induced inflammation: antioxidants as therapeutic agents in metabolic diseases, Int. J. Mol. Sci. 26 (17) (2025) 8544, https://doi.org/10.3390/ijms26178544.
[49] R.K. Semple, A. Sleigh, P.R. Murgatroyd, C.A. Adams, L. Bluck, S. Jackson, et al., Postreceptor insulin resistance contributes to human dyslipidemia and hepatic steatosis, J. Clin. Invest. 119 (2) (2009) 315–322, https://doi.org/10.1172/jci37432.
[50] J.L. Rains, S.K. Jain, Oxidative stress, insulin signaling, and diabetes, Free Radic. Biol. Med. 50 (5) (2011) 567–575, https://doi.org/10.1016/j.freeradbiomed.2010.12.006.
[51] F.M. Simabuco, M.G. Morale, I.C.B. Pavan, A.P. Morelli, F.R. Silva, R. E. Tamura, p53 and metabolism: from mechanism to therapeutics, Oncotarget 9 (34) (2018) 23780–23823, https://doi.org/10.18632/oncotarget.25267.
[52] B.S. Sayan, A.E. Sayan, R.A. Knight, G. Melino, G.M. Cohen, p53 Is cleaved by caspases generating fragments localizing to mitochondria, J. Biol. Chem. 281 (19) (2006) 13566–13573, https://doi.org/10.1074/jbc.m512467200.
[53] A.I. Legaki, I.I. Moustakas, M. Sikorska, G. Papadopoulos, R.I. Velliou, A. Chatzigeorgiou, Hepatocyte mitochondrial dynamics and bioenergetics in obesity-related non-alcoholic fatty liver disease, Curr. Obes. Rep. 11 (3) (2022) 126–143, https://doi.org/10.1007/s13679-022-00473-1.
[54] J.R. Moffett, N. Puthillathu, R. Vengilote, D.M. Jaworski, A. M. Namboodiri, Acetate revisited: a key biomolecule at the nexus of metabolism, epigenetics and oncogenesis-part 1: acetyl-CoA, acetogenesis and acyl-CoA short-chain synthetases, Front. Physiol. 11 (2020) 580167, https://doi.org/10.3389/fphys.2020.580167.

[55] J. Wang, Y. Wen, W. Zhao, Y. Zhang, F. Lin, C. Ouyang, et al., Hepatic conversion of acetyl-CoA to acetate plays crucial roles in energy stress, Elife 12 (2023). RP87419.
[56] X. Ou, M.R. Lee, X. Huang, S. Messina-Graham, H.E. Broxmeyer, SIRT1 positively regulates autophagy and mitochondria function in embryonic stem cells under oxidative stress, Stem Cells 32 (5) (2014) 1183–1194, https://doi.org/10.1002/stem.1641.
[57] X. Pan, S. Mota, B. Zhang, Circadian clock regulation on lipid metabolism and metabolic diseases, Adv. Exp. Med. Biol. 1276 (2020) 53–66, https://doi.org/10.1007/978-981-15-6082-8_5.
[58] J. Wang, M. Cao, S. Li, W. Pei, J. Li, Z. Wang, Circadian clock genes: their influence on liver metabolism, disease development and treatment (review), Mol. Med. Rep. 33 (1) (2025) 3, https://doi.org/10.3892/mmr.2025.13713.
[59] M. Young, G. McGinnis, Circadian regulation of metabolic homeostasis: causes and consequences, Nat. Sci. Sleep. 8 (2016) 163–180, https://doi.org/10.2147/nss.s78946.
[60] D.T. Rutkowski, S.M. Arnold, C.N. Miller, J. Wu, J. Li, K.M. Gunnison, K. Mori, et al., Adaptation to ER stress is mediated by differential stabilities of pro-survival and pro-apoptotic mRNAs and proteins, PLoS Biol 4 (11) (2006) e374, https://doi.org/10.1371/journal.pbio.0040374.
[61] C. Hetz, K. Zhang, R.J. Kaufman, Mechanisms, regulation and functions of the unfolded protein response, Nat. Rev. Mol. Cell. Biol. 21 (8) (2020) 421–438, https://doi.org/10.1038/s41580-020-0250-z.
[62] C. Lebeaupin, D. Vallée, Y. Hazari, C. Hetz, E. Chevet, B. Bailly-Maitre, Endoplasmic reticulum stress signalling and the pathogenesis of non-alcoholic fatty liver disease, J. Hepatol. 69 (4) (2018) 927–947, https://doi.org/10.1016/j.jhep.2018.06.008.
[63] Q. Lu, X. Tian, H. Wu, J. Huang, M. Li, Z. Mei, et al., Metabolic changes of hepatocytes in NAFLD, Front. Physiol. 12 (2021) 710420, https://doi.org/10.3389/fphys.2021.710420.